Inorganic Chemistry

pubs.acs.org/IC Article

# Engineering a Highly Improved Porous Photocatalyst Based on $Cu_2O$ by a Synergistic Effect of Cation Doping of Zn and Carbon Layer Coating

Yusheng Yuan,[‖] Li-ming Sun,[‖] Hao Gao,[‖] Sha Mo, Tianyi Xu, Lei Yang, and Wen-Wen Zhan*

Cite This: https://dx.doi.org/10.1021/acs.inorgchem.0c02547 Read Online

ACCESS | Metrics & More | Article Recommendations | Supporting Information

**ABSTRACT:** Zn-doped cuprous oxide ($Cu_2O$) nanoparticles coated by carbon layers ($Zn/Cu_2O@C$) have been obtained via a bimetallic MOF (Zn/Cu-MOF-199) as the sacrificial precursor. Originated from the octahedral morphology of Zn/Cu-MOF-199, the as-synthesized $Zn/Cu_2O@C$ shows a porous octahedron structure. The obtained $Zn/Cu_2O@C$ can afford the following merits. (1) The cation doping of Zn inside $Cu_2O$ can enhance the light absorption by introducing impurity energy levels and facilitate the separation of photoinduced electrons and holes. (2) The coating of a carbon layer in $Zn/Cu_2O@C$ can also efficiently enhance the separation efficiency of photoinduced charge carriers. (3) The porous structure of $Zn/Cu_2O@C$ can provide increased active sites. Therefore, these merits lead to the highly improved photocatalytic activities toward various chemical reactions. In addition, the fully coated carbon layer can facilitate the cycle stability of $Zn/Cu_2O@C$ in the photocatalytic processes.

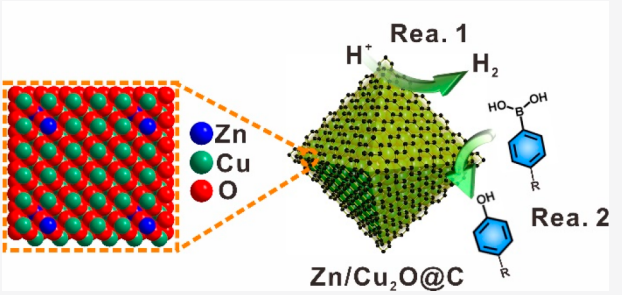


## 1. INTRODUCTION

Cuprous oxide ($Cu_2O$) has high potentials in the field of photocatalysis, due to its narrow band gap, higher hole mobility, and longer carrier diffusion length path.[1] With a direct band gap of 2.17 eV, $Cu_2O$ can act as a photocatalyst of visible-light-induced chemical reactions. Moreover, previous reports have demonstrated that suitable cation doping in $Cu_2O$ can tune the energy levels and decrease the band gap, leading to the enhanced light absorption ability.[2] However, the photocatalytic activity of $Cu_2O$ has been limited due to the relatively lower separation efficiency of photoinduced charge carriers and the instability related with the intermediate valence state of Cu(I) and photocorrosion issues.[3] Engineering heterostructures based on doped $Cu_2O$ and other materials (such as $TiO_2$, ZnO, and metal), which can provide a separation path for the photoinduced electrons and holes, may be able to solve the above issues.[4] Nevertheless, studies on fabricating a material which can combine the merits of cation doping and heterostructures have not been given sufficient attention due to the difficulties in the rational design of such materials.

According to an experimental and theoretical investigation reported previously, cation doping of Zn in $Cu_2O$ can modulate the energy band structure by forming impurity levels and can affect the electrical characteristics of the entire system, resulting in the improved performances for photocatalysis and photoelectrochemistry.[5] Except for the semiconductors (such as $TiO_2$) that can match well with the energy band of $Cu_2O$ and control the transfer path of photoinduced charge carriers, carbon materials with high mobility of charge carriers and low cost can be an ideal alternative to noble metals and can lead to the highly enhanced separation efficiency of photoinduced charge carriers when forming heterostructures with $Cu_2O$ as the photocatalysts.[6] Also, the fully coated carbon layer on $Cu_2O$ can help avoid the redox reaction of Cu(I), and the controlled transfer of photoinduced electrons from $Cu_2O$ to the carbon layer can relieve the photocorrosion issue. Based on the above analysis, $Cu_2O$-based composites with the cation doping of Zn and coating of carbon layers are expected to demonstrate highly improved photocatalytic activities and stability; however, as far as we know, such materials are seldom reported, although the cation doping of Zn has been obtained via different methods due to the similar radius of $Zn^{2+}$ and $Cu^{+}$.[7]

Recently, metal−organic frameworks (MOFs), especially bimetallic MOFs, composed of tunable metal cations and organic ligands, have attracted numerous attention as the annealing precursors of various functional composites.[8] Owning to the great advantages originating from the orderly

Received: August 26, 2020






https://dx.doi.org/10.1021/acs.inorgchem.0c02547
Inorg. Chem. XXXX, XXX, XXX−XXX

**Scheme 1. Schematic Illustration of the Synthetic Process of a Zn/$Cu_2O$@C Octahedron**

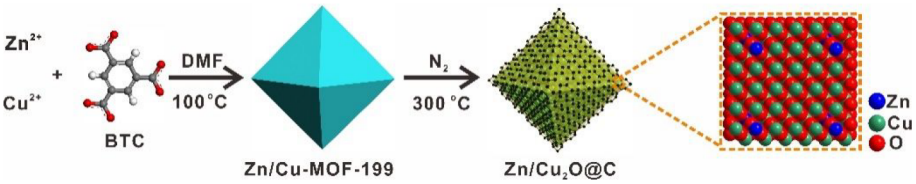


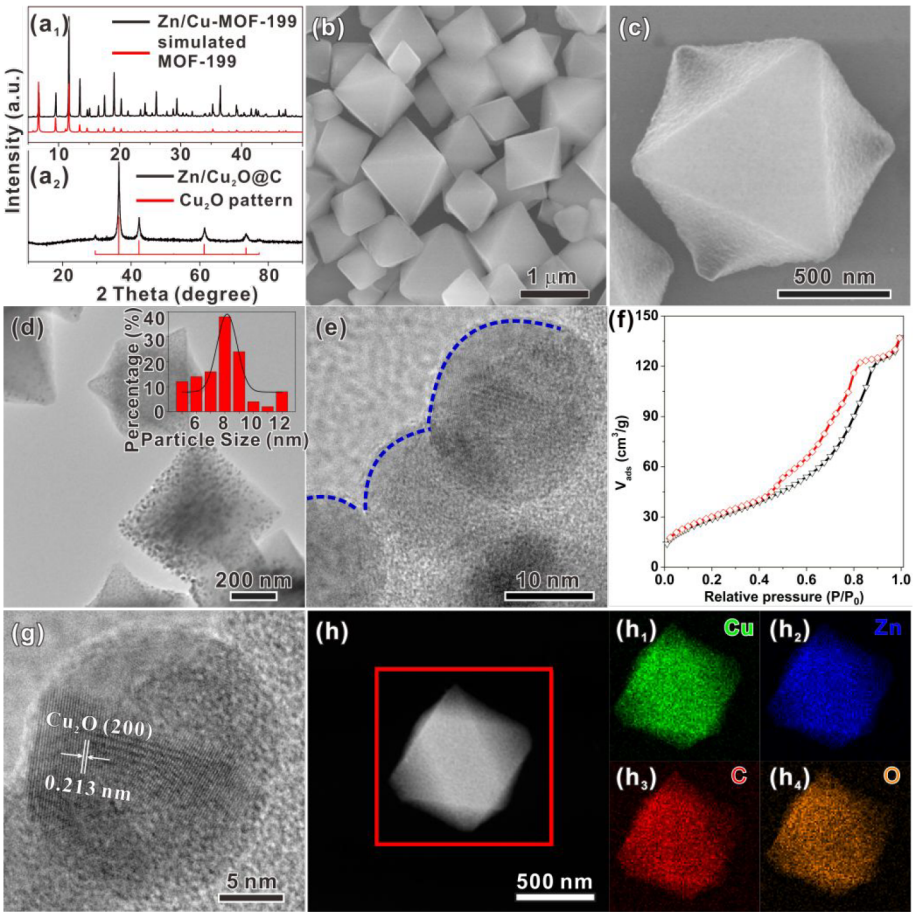


**Figure 1.** Powder XRD patterns of ($a_1$) Zn/Cu-MOF-199 octahedral nanoparticles and ($a_2$) Zn/$Cu_2O$@C obtained by calcining Zn/Cu-MOF-199 octahedral nanoparticles. (b) Typical SEM image and (c) high-magnification SEM image of the obtained Zn/$Cu_2O$@C. (d) Lower-magnification TEM images of Zn/$Cu_2O$@C. Inset of (d) is the corresponding particle size distribution of the Zn/$Cu_2O$ nanoparticles. (e) High-magnification TEM image of Zn/$Cu_2O$@C. (f) $N_2$ soprtion curves of Zn/$Cu_2O$@C. (g) High-resolution TEM image of Zn/$Cu_2O$@C. (h) HADDF-STEM image of a single Zn/$Cu_2O$@C particle and its corresponding element mapping profiles.

porous structure and molecular dispersion of metal cations and organic ligands in parent MOFs, these derivatives have shown significant potentials in many fields related to energy conversion.[9] Therefore, according to the structural features of $Cu_2O$-based composites that we mentioned above, we have chosen Zn/Cu bimetallic MOFs (Zn/Cu-MOF-199) as the precursors to fabricate the target material. Due to the molecular dispersion of Zn and Cu in the bimetallic MOF precursor, we have successfully fabricated a porous octahedron structure composed of carbon layer-coated Zn-doped $Cu_2O$ nanoparticles (Zn/$Cu_2O$@C). As expected, the obtained Zn/$Cu_2O$@C octahedra have shown improved photocatalytic activities toward various reaction systems, due to the beneficial structural features of cation doping of Zn, the carbon layer coating, and the porous structure, which can not only enhance the light absorption ability and separation efficiency of photoinduced charge carriers but also create more active sites. Moreover, the carbon layer coating can facilitate the stability of Zn/$Cu_2O$@C in the photocatalytic processes, leading to good cycle stability after five evaluation processes of the hydrogen generation reaction.

## 2. RESULTS AND DISCUSSION

As shown in Scheme 1, bimetallic Zn/Cu-MOF-199 has been obtained via a solvothermal strategy with $Zn^{2+}$ and $Cu^{2+}$ as the bimetallic resources. After the calcination process under $N_2$ atmosphere, the Zn/Cu-MOF-199 precursors can be converted into Zn-doped $Cu_2O$ coated by carbon layers. The typical scanning electron microscopy (SEM) image (Figure S1a) indicates that the precursor Zn/Cu-MOF-199 has a uniform octahedral morphology with smooth surfaces and an average particle size of about 1.3 $\mu$m (Figure S1b). The corresponding XRD pattern (Figure 1$a_1$) in Figure 1 shows


https://dx.doi.org/10.1021/acs.inorgchem.0c02547
Inorg. Chem. XXXX, XXX, XXX−XXX

only the peaks assigned to MOF-199.[10] Energy-dispersive X-ray spectroscopy (EDS) results, including the elemental mapping shown in Figure S2, verify the existence and the uniform distribution of Zn and Cu elements in the obtained octahedral nanoparticles, indicating the successful doping of Zn element in the Cu-MOF-199 crystalline structure. According to the thermogravimetric analysis (TGA, Figure S3) of the Zn/Cu-MOF-199, the annealing temperature has been set at 300 °C to ensure the complete conversion of MOF structure to its derivative. After the calcination treatment, the low- and high-magnification SEM images (Figure 1b and c) of the obtained sample show a well-maintained octahedral morphology, though with rough surfaces and a smaller size distribution (about 1.1 mm, Figure S1b). The XRD pattern (Figure 1a$_2$) of the derivative shows only peaks assigned to $Cu_2O$, indicating the possibility of the doping of Zn inside the $Cu_2O$ crystalline structure. According to the XRD pattern, no obvious shift of peaks is observed in Zn/$Cu_2O$@C after the atomic doping, and this phenomenon has also been reported by other studies on Zn-doped $Cu_2O$.[5] In order to explain this phenomenon, we have simulated the XRD pattern of the $Cu_2O$ crystal structure with one Cu atom replaced by Zn (Figure S4), which shows no shift, confirming the possibility of no shift in the XRD peaks after the atomic doping.

The transmission electron microscopy (TEM) image has also been investigated to obtain more detailed structure information on Zn/$Cu_2O$@C. The low- and high-magnification TEM images (Figures 1d and 1e) of Zn/$Cu_2O$@C octahedral particles show that the octahedral particles have a porous structure composed of large amounts of nanoparticles surrounded by carbon layers. The size distribution curve of the nanoparticles inside Zn/$Cu_2O$@C gives an average size of about 11.5 nm. The existence of a carbon layer has been further revealed by Raman spectroscopy (Figure S5), which shows the characteristic peaks of graphic carbon, i.e., a D band and G band. The porous structure can be revealed by $N_2$ sorption measurement (Figures 1f and S6), which provides a large BET surface area of 108.1 $m^2/g$, and the pore size distribution mainly centers at the range of 1−10 nm, which can be attributed to the accumulation of the nanoparticles. A further high-resolution TEM image (Figure 1g) displays the crystal fringe spacing of 0.213 nm in a monodispersed nanoparticle, which can be assigned to the (200) planes of $Cu_2O$. The corresponding selected area electron diffraction (SAED) pattern displays a set of concentric rings, which also matches well with $Cu_2O$ phase (Figure S7). The doping of Zn can be confirmed by the elemental mapping of the Zn/$Cu_2O$@C shown in Figure 1h−h$_4$, where the Cu, Zn, O, and C elements are uniformly distributed. ICP (inductively coupled plasma) results of Zn/$Cu_2O$@C provides an accurate mass fraction of Zn as 4.07%, and the calculated ratio of Zn/Cu is about 8.2%. According to the above results, the annealing product, Zn/$Cu_2O$@C, has a porous octahedral structure composed of carbon layer-coated Zn-doped $Cu_2O$ nanoparticles.

X-ray photoelectron spectroscopy (XPS, Figure 2) has been utilized to investigate the chemical states of elements in Zn/$Cu_2O$@C and to confirm the doping of Zn inside $Cu_2O$. The survey spectrum (Figure 2a) has demonstrated the coexistence of Cu, Zn, O, and C elements in the obtained Zn/$Cu_2O$@C. The high-resolution O 1s and C 1s spectrum of Zn/$Cu_2O$@C is shown in Figure S8. The high-resolution Cu 2p spectrum shown in Figure 2b displays two sets of peaks assigned to $Cu^+$

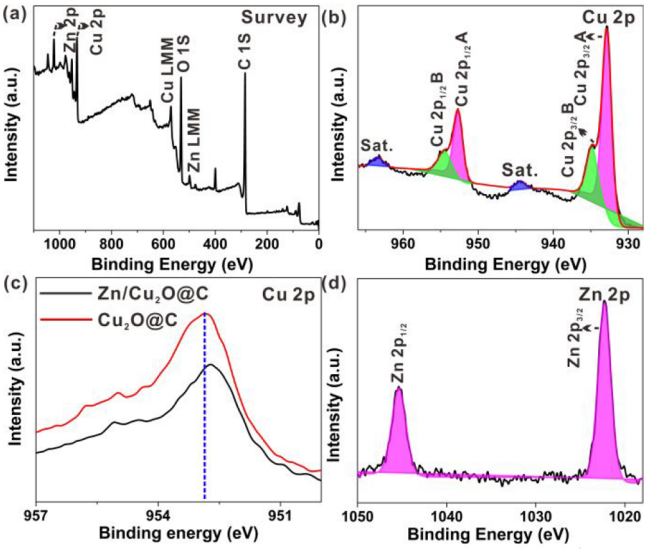


**Figure 2.** (a) XPS survey and high-resolution (b) Cu 2p spectrum of Zn/$Cu_2O$@C particles. (c) Comparison of Cu 2p spectra between Zn/$Cu_2O$@C and $Cu_2O$@C. (d) High-resolution Zn 2p spectrum of Zn/$Cu_2O$@C.

(932.5 and 952.33 eV) and $Cu^{2+}$ (934.6 eV, 954.3 eV, and satellite peaks), where the $Cu^+$ should be attributed to $Cu_2O$ and the $Cu^{2+}$ should be attributed to the surface oxidation of $Cu_2O$ to CuO. There is only one peak at 916.6 eV ($Cu^+$) in the Auger Cu LMM curve of Zn/$Cu_2O$@C (Figure S9), confirming the main formation of Cu element as $Cu_2O$. As shown in Figure 2c, there is an obvious red shift of the Cu 2p spectrum in Zn/$Cu_2O$@C compared with undoped $Cu_2O$@C (obtained by pure Cu-MOF-199 as the precursor, Figures S10 and S11), which should be attributed from copper-deficient regions inside $Cu_2O$ caused by cation doping of Zn.[5] The high-resolution Zn 2p spectrum shows peaks assigned to $Zn^{2+}$ (Figure 2d), confirming the cation doping of Zn inside $Cu_2O$.

The photocatalytic performance (shown in Figure 3) of Zn/$Cu_2O$@C with the structural features of cation doping of Zn and coating carbon layer has been first evaluated by the hydrogen evolution reaction from water. As shown in Figure 3a and 3b, Zn/$Cu_2O$@C can afford a hydrogen evolution rate of 26 $\mu$mol/g/h and shows a good stability during the five cycles of photocatalytic processes under the irradiation of simulated solar light. Compared with contrast samples with different doping amounts of Zn, including $Cu_2O$@C, Zn/$Cu_2O$@C-*l* (*l* represents less doping amount of Zn), and Zn/$Cu_2O$@C-*m* (*m* represents more doping amount of Zn) (see details in Figures S10−S12 and Tables S1 and S2), Zn/$Cu_2O$@C has shown a much higher activity toward the hydrogen evolution reaction during the reaction time of 10 h due to the optimized amount of cation doping. Zn/$Cu_2O$@C-*l* and Zn/$Cu_2O$@C have shown highly enhanced activity than undoped $Cu_2O$@C, while Zn/$Cu_2O$@C-*m* has shown decreased photocatalytic activity (Figure 3a and Figure S13), indicating the positive influence of doping Zn in $Cu_2O$, though there is a limitation for the doping amount. Nevertheless, the stability of calcination products with different doping amounts of Zn has been maintained well after five cycles and without obvious decrease in the hydrogen evolution rate (Figure S14). Moreover, the positive influences of carbon layers on both the activity and stability have been highlighted by the significantly decreased separation efficiency of photoinduced charge carriers, the hydrogen generation rate


https://dx.doi.org/10.1021/acs.inorgchem.0c02547
Inorg. Chem. XXXX, XXX, XXX−XXX

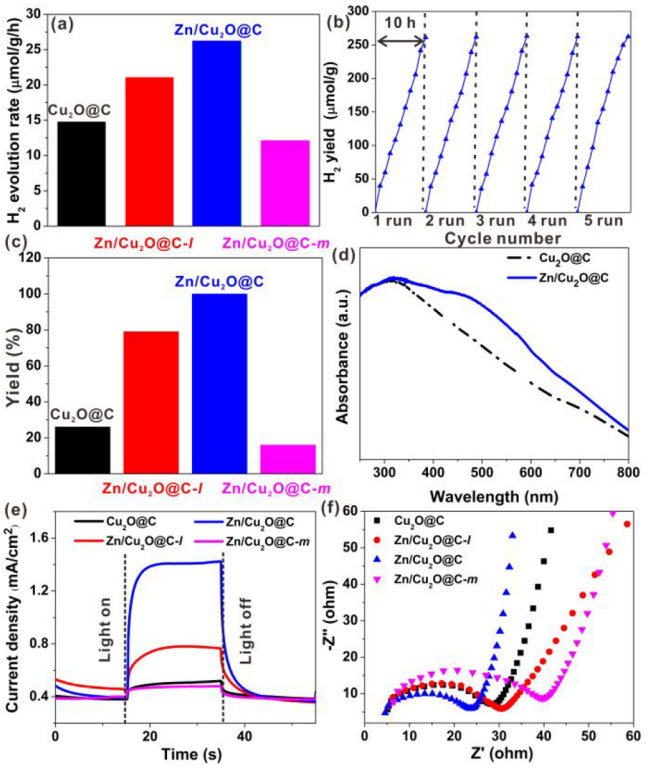


**Figure 3.** (a) Simulated solar light-induced hydrogen evolution rates from water over different photocatalysts. (b) Typical time course curves of hydrogen yield with Zn/$Cu_2O$@C as the photocatalyst for five cycles with an interval of 10 h. (c) Yields of 4-methoxyphenol via the oxidative hydroxylation of arylboronic acids over various photocatalysts under irradiation of blue LED light. (d) UV−vis spectra of $Cu_2O$@C and Zn/$Cu_2O$@C. (e) Photocurrent density measurement and (f) electrochemical impedance spectroscopy represented by the Nyquist plots of the various catalyst samples.

of Zn/$Cu_2O$ (Figures S15−S17), and the obvious blue color of the reaction solution containing Zn/$Cu_2O$ after the catalytic process, which should be caused by the dissolution of $Cu_2O$ in the aqueous solution containing 2-hydroxypropanoic acid (HL) (Figure S18). By contrast, there has been no obvious blue color in the reaction solution containing Zn/$Cu_2O$@C (Figure S18c). The characterization of the Zn/$Cu_2O$@C after the catalysis also indicates the good stability during the catalytic processes (Figure S19). In addition, the obtained Zn/$Cu_2O$@C can also demonstrate enhanced activity toward the visible-light-induced reaction, e.g., the hydroxylation of phenylboric acids (Figure 3c and Table S3). Zn/$Cu_2O$@C as the photocatalyst can afford almost 100% yield of 4-methoxyphenol at a reaction time of 8 h, which is much higher than those of the undoped $Cu_2O$@C and other control samples, further indicating the optimized doping amount of Zn in Zn/$Cu_2O$@C.

Thorough investigation for the influences of doping Zn on the photocatalytic activity of $Cu_2O$ has been taken by the characterizations of UV−vis spectra, photocurrent density measurement, linear sweep voltammetry (LSV), and electrochemical impedance spectroscopy (EIS). Zn/$Cu_2O$@C has an obviously higher adsorption at the visible-light region than $Cu_2O$@C, and the broad peak at about 500 nm can be assigned to the impurity level induced by cation doping of Zn (Figure 3d). Photocurrent density curves of the various catalysts with different doping amounts of $Zn^{2+}$ (Figure 3e) have been obtained at the condition with a voltage of 0.35 V and on−off intervals of 20 s. The trend of photocurrent density values follows the same order with the photocatalytic activities of the four catalysts; Zn/$Cu_2O$@C has the highest photocurrent density, indicating its much faster separation efficiency of photoinduced electrons and holes, while the decreased photocurrent response of Zn/$Cu_2O$@C-*m* indicates that the excessive doping of Zn can lead to the rapid recombination of the electrons and holes. This phenomenon can be assigned to the interstitial energy levels induced confrontational relationship between the light absorption enhancement and carrier migration efficiency decrease, which is responsible for the activity trend among the samples with various Zn amounts. In addition, Zn/$Cu_2O$@C has the smallest semicircular radius in the Nyquist plot (Figure 3f), which further reveals the more effective separation of photoinduced charge transfer after the doping of Zn in $Cu_2O$. LSV curves indicate that Zn/$Cu_2O$@C has the highest cathodic current density for the reduction of water to $H_2$ among the four photocatalysts (Figure S20). All of the above results have indicated that the controlled doping of Zn in $Cu_2O$ can facilitate light absorption and the separation of photoinduced electrons and holes, making Zn/$Cu_2O$@C as the optimized photocatalyst for various reactions.

## 3. CONCLUSIONS

With Zn/Cu-MOF-199 octahedral nanoparticles as the sacrificial template, carbon layer-coated Zn-doped $Cu_2O$ nanoparticles (about 11.5 nm) assembled into porous octahedra have been obtained. The as-synthesized Zn/$Cu_2O$@C has shown highly improved photocatalytic activities toward the hydrogen evolution reaction and visible-light induced hydroxylation of phenylboric acids. The synergistic effect of carbon layer and cation doping of Zn in $Cu_2O$ leads to the effectively enhanced light absorption and separation efficiency of photoinduced charge carriers, and the larger surface area of Zn/$Cu_2O$@C leads to more active sites, which are responsible for the good photocatalytic activities of Zn/$Cu_2O$@C. Moreover, Zn/$Cu_2O$@C has shown excellent cycle stability in photocatalytic processes. This report here may open a new avenue in fabricating $Cu_2O$-based photocatalysts with excellent performances.

## ■ ASSOCIATED CONTENT

### Supporting Information

The Supporting Information is available free of charge at https://pubs.acs.org/doi/10.1021/acs.inorgchem.0c02547.

SEM image of the Zn/Cu-MOF-199 precursor and particle size distribution of the samples (Figure S1); EDS and TGA measurement of Zn/Cu-MOF-199 (Figures S2 and S3); calculated XRD pattern of Zn/$Cu_2O$ (Figure S4); Raman spectrum, pore size distribution, and XPS spectra of Zn/$Cu_2O$@C (Figures S5−S9); SEM images, XRD patterns, and EDS data of the Zn/Cu-MOF-199 with various Zn amounts and their derivatives (Figures S10−S12, Tables S1 and S2); comparison in the quantum efficiency and stability of the various samples (Figures S13 and S14); characterization of Zn/$Cu_2O$ (Figure S15); comparison in the photocurrent response between Zn/$Cu_2O$@C and Zn/$Cu_2O$ (Figure S16); hydrogen evolution data of Zn/$Cu_2O$ (Figures S17 and S18); characterization of Zn/$Cu_2O$@C after the catalytic test (Figure S19); control


https://dx.doi.org/10.1021/acs.inorgchem.0c02547
Inorg. Chem. XXXX, XXX, XXX−XXX

experiments (Table S3); and LSV curves of various samples (Figure S20) (PDF)

## AUTHOR INFORMATION


### Corresponding Author

**Wen-Wen Zhan** − *Jiangsu Key Laboratory of Green Synthetic Chemistry for Functional Materials, Department of Chemistry, School of Chemistry and Chemical Engineering, Jiangsu Normal University, Xuzhou 221116, P. R. China;* orcid.org/0000-0002-7004-9155; Email: wwzhan@jsnu.edu.cn

### Authors

**Yusheng Yuan** − *Jiangsu Key Laboratory of Green Synthetic Chemistry for Functional Materials, Department of Chemistry, School of Chemistry and Chemical Engineering, Jiangsu Normal University, Xuzhou 221116, P. R. China*

**Li-ming Sun** − *Jiangsu Key Laboratory of Green Synthetic Chemistry for Functional Materials, Department of Chemistry, School of Chemistry and Chemical Engineering, Jiangsu Normal University, Xuzhou 221116, P. R. China*

**Hao Gao** − *Jiangsu Key Laboratory of Green Synthetic Chemistry for Functional Materials, Department of Chemistry, School of Chemistry and Chemical Engineering, Jiangsu Normal University, Xuzhou 221116, P. R. China*

**Sha Mo** − *Jiangsu Key Laboratory of Green Synthetic Chemistry for Functional Materials, Department of Chemistry, School of Chemistry and Chemical Engineering, Jiangsu Normal University, Xuzhou 221116, P. R. China*

**Tianyi Xu** − *Jiangsu Key Laboratory of Green Synthetic Chemistry for Functional Materials, Department of Chemistry, School of Chemistry and Chemical Engineering, Jiangsu Normal University, Xuzhou 221116, P. R. China*

**Lei Yang** − *Shenzhen HUASUAN Technology Co., Ltd., Shenzhen 518055, P. R. China*

Complete contact information is available at: https://pubs.acs.org/10.1021/acs.inorgchem.0c02547


### Author Contributions

[‖]These authors contributed equally. W.W.Z. conceived and designed the experiments and cowrote the paper. Y.S.Y., L.M.S., and H.G. performed most of the experiments. The manuscript was written through contributions of all authors. All authors have given approval to the final version of the manuscript.

### Notes

The authors declare no competing financial interest.

## ACKNOWLEDGMENTS

This work was supported by the National Natural Science Foundation of China (21701063, 21671085), the Natural Science Foundation of Jiangsu Province (BK20191466), the Top-notch Academic Programs Project of Jiangsu Higher Education Institutions (TAPP), the Postgraduate Research and Practical Innovation Program of Jiangsu Province (KYCX20_2244), and the Project Funded by the Priority Academic Program Development of Jiangsu Higher Education Institutions.

## REFERENCES

(1) Fu, Y.; Li, Q.; Liu, J.; Jiao, Y.; Hu, S.; Wang, H.; Xu, S.; Jiang, B. In-situ chemical vapor deposition to fabricate Cuprous oxide/copper sulfide core-shell flowers with boosted and stable wide-spectral region photocatalytic performance. *J. Colloid Interface Sci.* **2020**, *570*, 143−152. Huang, L.; Peng, F.; Yu, H.; Wang, H. Preparation of cuprous oxides with different sizes and their behaviors of adsorption, visible-light driven photocatalysis and photocorrosion. *Solid State Sci.* **2009**, *11*, 129−138. Wang, Y.; Huang, D.; Zhu, X.; Ma, Y.; Geng, H.; Wang, Y.; Yin, G.; He, D.; Yang, Z.; Hu, N. Surfactant-free synthesis of $Cu_2O$ hollow spheres and their wavelength-dependent visible photocatalytic activities using LED lamps as cold light sources. *Nanoscale Res. Lett.* **2014**, *9*, 624.

(2) Lee, K.; Lee, C.-H.; Cheong, J. Y.; Lee, S.; Kim, I.-D.; Joh, H.-I.; Lee, D. C. Expanding depletion region via doping: Zn-doped $Cu_2O$ buffer layer in $Cu_2O$ photocathodes for photoelectrochemical water splitting. *Korean J. Chem. Eng.* **2017**, *34*, 3214−3219. Martinez-Ruiz, A.; Moreno, M. G.; Takeuchi, N. First principles calculations of the electronic properties of bulk $Cu_2O$, clean and doped with Ag, Ni, and Zn. *Solid State Sci.* **2003**, *5*, 291−295.

(3) Mittiga, A.; Salza, E.; Sarto, F.; Tucci, M.; Vasanthi, R. Heterojunction solar cell with 2% efficiency based on a $Cu_2O$ substrate. *Appl. Phys. Lett.* **2006**, *88*, 163502. Jung, K.; Lim, T.; Bae, H.; Ha, J.-S.; Martinez-Morales, A. A. $Cu_2O$ Photocathode with Faster Charge Transfer by Fully Reacted Cu Seed Layer to Enhance Performance of Hydrogen Evolution in Solar Water Splitting Applications. *ChemCatChem* **2019**, *11*, 4377−4382.

(4) Wang, M.; Sun, L.; Lin, Z.; Cai, J.; Xie, K.; Lin, C. p-n Heterojunction photoelectrodes composed of $Cu_2O$-loaded $TiO_2$ nanotube arrays with enhanced photoelectrochemical and photocatalytic activities. *Energy Environ. Sci.* **2013**, *6*, 1211−1220. Liu, L.; Yang, W.; Sun, W.; Li, Q.; Shang, J. K. Creation of $Cu_2O$@$TiO_2$ Composite Photocatalysts with p-n Heterojunctions Formed on Exposed $Cu_2O$ Facets, Their Energy Band Alignment Study, and Their Enhanced Photocatalytic Activity under Illumination with Visible Light. *ACS Appl. Mater. Interfaces* **2015**, *7*, 1465−1476. Lou, Y.; Zhang, Y.; Cheng, L.; Chen, J.; Zhao, Y. A Stable Plasmonic Cu@$Cu_2O$/ZnO Heterojunction for Enhanced Photocatalytic Hydrogen Generation. *ChemSusChem* **2018**, *11*, 1505−1511. Sun, Y. G.; Cai, L. Y.; Liu, X. J.; Cui, Z.; Rao, P. H. Tailoring heterostructures of Ag/$Cu_2O$ hybrids for enhanced photocatalytic degradationdegradation. *J. Phys. Chem. Solids* **2017**, *111*, 75−81.

(5) Zhu, C. Q.; Panzer, M. J. Synthesis of Zn:$Cu_2O$ Thin Films Using a Single Step Electrodeposition for Photovoltaic Applications. *ACS Appl. Mater. Interfaces* **2015**, *7*, 5624−5628. Heng, B.; Xiao, T.; Tao, W.; Hu, X.; Chen, X.; Wang, B.; Sun, D.; Tang, Y. Zn Doping-Induced Shape Evolution of Microcrystals: The Case of Cuprous Oxide. *Cryst. Growth Des.* **2012**, *12*, 3998−4005.

(6) Han, X.; He, X.; Wang, F.; Chen, J.; Xu, J.; Wang, X.; Han, X. Engineering an N-doped $Cu_2O$@N-C interface with long-lived photogenerated carriers for efficient photoredox catalysts. *J. Mater. Chem. A* **2017**, *5*, 10220−10226. Wei, Q.; Wang, Y.; Qin, H. Y.; Wu, J. M.; Lu, Y. F.; Chi, H. Z.; Yang, F.; Zhou, B.; Yu, H. L.; Liu, J. B. Construction of rGO wrapping octahedral Ag-$Cu_2O$ heterostructure for enhanced visible light photocatalytic activity. *Appl. Catal., B* **2018**, *227*, 132−144.

(7) Nolan, M.; Elliott, S. D. Tuning the transparency of $Cu_2O$ with substitutional cation doping. *Chem. Mater.* **2008**, *20*, 5522−5531. Zhang, L.; Jing, D.; Guo, L.; Yao, X. In Situ Photochemical Synthesis of Zn-Doped $Cu_2O$ Hollow Microcubes for High Efficient Photocatalytic H-2 Production. *ACS Sustainable Chem. Eng.* **2014**, *2*, 1446−1452.

(8) Hao, J.; Zhan, W.; Sun, L.; Zhuang, G.; Wang, X.; Han, X. Combining N, S-Codoped C and $CeO_2$: A Unique Hinge-like Structure for Efficient Photocatalytic Hydrogen Evolution. *Inorg. Chem.* **2020**, *59*, 937−942. Zhan, W.; Yuan, Y.; Sun, L.; Yuan, Y.; Han, X.; Zhao, Y. Hierarchical NiO@N-Doped Carbon Microspheres with Ultrathin Nanosheet Subunits as Excellent Photocatalysts for Hydrogen Evolution. *Small* **2019**, *15*, 1901024. Fu, S.; Zhu, C.; Song, J.; Du, D.; Lin, Y. Metal-Organic Framework-Derived Non-Precious Metal Nanocatalysts for Oxygen Reduction Reaction. *Adv. Energy Mater.* **2017**, *7*, 1700363. Zhao, S.-N.; Song, X.-Z.; Song, S.-Y.; Zhang, H.-J. Highly efficient heterogeneous catalytic materials derived from

metal-organic framework supports/precursors. *Coord. Chem. Rev.* **2017**, *337*, 80−96. Zhang, Z.; Zhang, S.; Yao, Q.; Chen, X.; Lu, Z.-H. Controlled Synthesis of MOF-Encapsulated NiPt Nanoparticles toward Efficient and Complete Hydrogen Evolution from Hydrazine Borane and Hydrazine. *Inorg. Chem.* **2017**, *56*, 11938−11945. Shi, J.; Qiu, F.; Yuan, W.; Guo, M.; Lu, Z. H. Nitrogen-doped carbon-decorated yolk-shell CoP@FeCoP micro-polyhedra derived from MOF for efficient overall water splitting. *Chem. Eng. J.* **2021**, *403*, 126312.

(9) Cao, X.; Tan, C.; Sindoro, M.; Zhang, H. Hybrid micro-/nano-structures derived from metal-organic frameworks: preparation and applications in energy storage and conversion. *Chem. Soc. Rev.* **2017**, *46*, 2660−2677. Xia, W.; Mahmood, A.; Zou, R.; Xu, Q. Metal-organic frameworks and their derived nanostructures for electrochemical energy storage and conversion. *Energy Environ. Sci.* **2015**, *8*, 1837−1866. Dang, S.; Zhu, Q.-L.; Xu, Q. Nanomaterials derived from metal-organic frameworks. *Nat. Rev. Mater.* **2018**, *3*, 17075. Yuan, Y.; Sun, L.; Li, Y.; Zhan, W.; Wang, X.; Han, X. Synergistic Modulation of Active Sites and Charge Transport: N/S Co-doped C Encapsulated $NiCo_2O_4$/NiO Hollow Microrods for Boosting Oxygen Evolution Catalysis. *Inorg. Chem.* **2020**, *59*, 4080−4089. Wang, H.; Li, X.; Lan, X.; Wang, T. Supported Ultrafine NiCo Bimetallic Alloy Nanoparticles Derived from Bimetal-Organic Frameworks: A Highly Active Catalyst for Furfuryl Alcohol Hydrogenation. *ACS Catal.* **2018**, *8*, 2121−2128. Huang, Y.-Y.; Konnerth, H.; Yeh, J.-Y.; Prechtl, M. H. G.; Wen, C.-Y.; Wu, K. C. W. De novo synthesis of Cr-embedded MOF-199 and derived porous CuO/$CuCr_2O_4$ composites for enhanced phenol hydroxylation. *Green Chem.* **2019**, *21*, 1889−1894. Hong, W.; Kitta, M.; Xu, Q. Bimetallic MOF-Derived FeCo-P/C Nanocomposites as Efficient Catalysts for Oxygen Evolution Reaction. *Small Methods* **2018**, *2*, 1800214.

(10) Wang, Y.; Lu, Y.; Zhan, W.; Xie, Z.; Kuang, Q.; Zheng, L. Synthesis of porous $Cu_2O$/CuO cages using Cu-based metal-organic frameworks as templates and their gas-sensing properties. *J. Mater. Chem. A* **2015**, *3*, 12796−12803.



https://dx.doi.org/10.1021/acs.inorgchem.0c02547
*Inorg. Chem.* XXXX, XXX, XXX−XXX